

# Journal of Materials Chemistry C

Accepted Manuscript



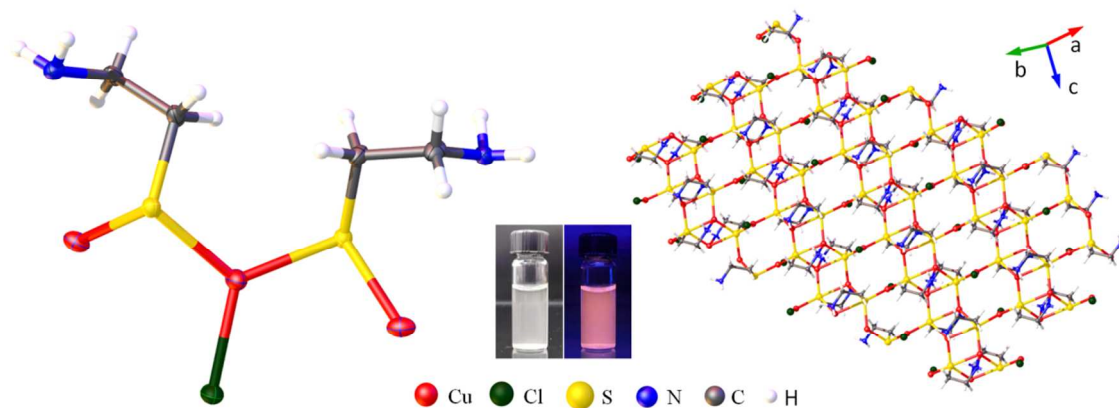
This is an *Accepted Manuscript*, which has been through the Royal Society of Chemistry peer review process and has been accepted for publication.

*Accepted Manuscripts* are published online shortly after acceptance, before technical editing, formatting and proof reading. Using this free service, authors can make their results available to the community, in citable form, before we publish the edited article. We will replace this *Accepted Manuscript* with the edited and formatted *Advance Article* as soon as it is available.

You can find more information about *Accepted Manuscripts* in the [Information for Authors](#).

Please note that technical editing may introduce minor changes to the text and/or graphics, which may alter content. The journal's standard [Terms & Conditions](#) and the [Ethical guidelines](#) still apply. In no event shall the Royal Society of Chemistry be held responsible for any errors or omissions in this *Accepted Manuscript* or any consequences arising from the use of any information it contains.

## TOC



We report the structure and optical properties of a new Cu-Cyteamine complex with formula of  $\text{Cu}_3\text{Cl}(\text{SR})_2$  ( $\text{R} = \text{CH}_2\text{CH}_2\text{NH}_2$ ), which shows intensive luminescence by UV or X-ray excitation.

Cite this: DOI: 10.1039/c0xx00000x

www.rsc.org/xxxxxx

## ARTICLE TYPE

**A new Cu-Cysteamine Complex: Structure and Optical Properties****Lun Ma<sup>a</sup>, Wei Chen<sup>a\*</sup>, Gabriele Schatte<sup>b</sup>, Wei Wang<sup>c</sup>, Alan G. Joly<sup>d</sup>, Yining Huang<sup>e</sup>, Ramaswami Sammynaiken<sup>b</sup>, and Marius Hossu<sup>a</sup>***Received (in XXX, XXX) Xth XXXXXXXXX 20XX, Accepted Xth XXXXXXXXX 20XX*

DOI: 10.1039/b000000x

Here we report the structure and optical properties of a new Cu-Cyteamine complex (Cu-Cy) with formula of  $\text{Cu}_3\text{Cl}(\text{SR})_2$  ( $\text{R} = \text{CH}_2\text{CH}_2\text{NH}_2$ ). This Cu-Cy has different structure from previous Cu-Cy in which both thio and amine groups from cysteamine bond with copper ions. Single-crystal X-ray diffraction and the solid-state nuclear magnetic resonance results show that the oxidation state of copper in the  $\text{Cu}_3\text{Cl}(\text{SR})_2$  is +1, rather than +2. Further, the  $\text{Cu}_3\text{Cl}(\text{SR})_2$  has been found with intense photoluminescence and X-ray excited luminescence. More interesting is that the  $\text{Cu}_3\text{Cl}(\text{SR})_2$  particles can produce singlet oxygen under irradiation by light or X-ray. This indicates that the  $\text{Cu}_3\text{Cl}(\text{SR})_2$  is a new photosensitizer that can be used for deep cancer treatment as X-ray can deeply penetrate soft tissues. All these mean that the  $\text{Cu}_3\text{Cl}(\text{SR})_2$  is a new material with potential applications for lighting, radiation detection and cancer treatment.

**Introduction**

Metal complexes have a long history, but started to attract much attention in modern science and industry since the middle of 19<sup>th</sup> century. As an important group in this family, transition metal complexes show novel structures, properties and applications.<sup>1-7</sup> Among those ligands, Cysteamine or 2-aminoethanethiol ( $\text{HSCH}_2\text{CH}_2\text{NH}_2$ ), a small organic molecule with both active thiol and amino groups, performs various physiological functions in the human body and is also used as a drug for several diseases.<sup>8, 9</sup> Its strong metal affinity has promoted interesting chemistry with many transition metals.<sup>10-16</sup> Copper is an essential metal element in living organisms. It can bind to sulfur ligand of proteins and is also found in many enzymes. Copper-Cysteamine (Cu-Cy) complexes could thus be considered as suitable model compounds in fundamental understandings of copper containing enzymes.<sup>17</sup> In general, Cu-Cy complexes can be obtained simply through green chemistry process with no harm to environment as cysteamine is nontoxic and soluble in water. Various Cu-Cy complexes have been studied and different crystal structures can even be obtained by changing reaction conditions.

Previous Cu-Cy complex crystals were usually obtained at room temperature and needed long time for crystal growth.<sup>18, 19</sup> In this work, we report a new Cu-Cy complex  $\text{Cu}_3\text{Cl}(\text{SR})_2$  ( $\text{R} = \text{CH}_2\text{CH}_2\text{NH}_2$ ) [hereafter referred as  $\text{Cu}_3\text{Cl}(\text{SR})_2$ ] using rapid high temperature growth. The structure is much simpler and both thiol group and amine group bond with Cu ion, which is different from previous Cu-Cy crystal structures.<sup>18, 19</sup> It may provide new

understandings in Cu-Cy formation. In addition, the  $\text{Cu}_3\text{Cl}(\text{SR})_2$  has intense luminescence while no luminescence has been reported in previous Cu-Cy complexes.<sup>18, 19</sup> It is particularly interesting that the  $\text{Cu}_3\text{Cl}(\text{SR})_2$  has strong luminescence when excited by X-ray. This means the compound not only can be used for lighting but also can be used for radiation detection and as a light source for X-ray induced photodynamic therapy on cancer treatment.<sup>20</sup> Even more interestingly, the  $\text{Cu}_3\text{Cl}(\text{SR})_2$  may produce singlet oxygen upon activation by light or X-ray. This makes it a new type of photosensitizer that can be used for both skin and deep cancer treatments which are described in a forthcoming article.<sup>20</sup>

**Results and discussion****Synthesis**

The majority of the crystals are rectangular shaped and their size ranges from about 3 to 10  $\mu\text{m}$  as shown in Figure 1 (a, b) by scanning electron microscopy (SEM). Larger crystals (Figure 1 c, d) are formed when stirring of the reaction mixture is not applied to prevent the interruption of the crystal growth process.

In addition to the micron-sized crystals, smaller crystals from tens to several hundred nanometers are also observed. Figure 2a shows the high resolution transmission electron microscopy (HRTEM) images of the small crystals. Their electron diffraction pattern (Figure 2b) suggests that these small crystals are single crystals. Further HRTEM images display their continuous

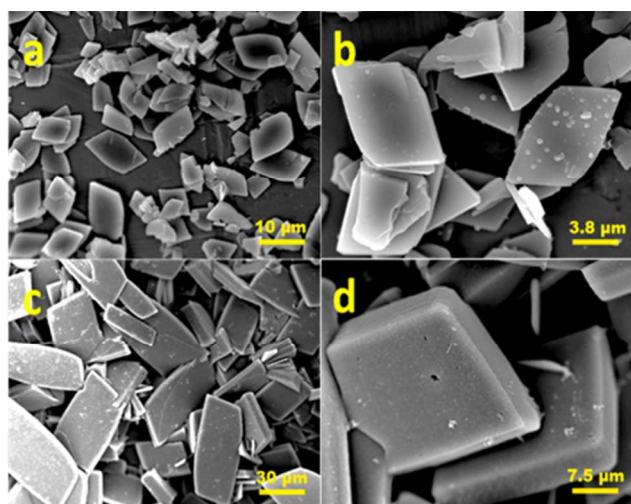


Figure 1. SEM images of  $\text{Cu}_3\text{Cl}(\text{SR})_2$  crystals. Small crystals are obtained with stirring (a, b). Larger crystals are obtained without stirring (c, d).

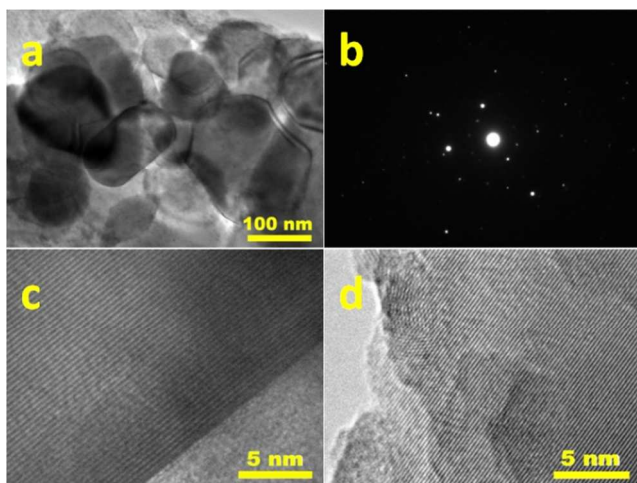


Figure 2. HRTEM images of very small crystals of  $\text{Cu}_3\text{Cl}(\text{SR})_2$  (a, c, and d). The image b is the electron diffraction pattern of the crystals.

uniform lattice fringes (Figure 2c, 2d). The small crystals can also form aggregates and have been observed as small spherical bumps attached to the large crystal surfaces. The HRTEM images demonstrate that these small crystals are highly crystalline and about 70 to 200 nm in size. The lattice spacings measured from the images are  $d_1 = 0.347$  nm (Figure 2c) and  $d_2 = 0.227$  nm (Figure 2d), respectively.

The powder XRD pattern of  $\text{Cu}_3\text{Cl}(\text{SR})_2$  displays very sharp and intense peaks (Figure 3). This is consistent with the HRTEM and SEM observations that the particles are highly crystalline and relatively large. The lattice spacing calculated from the XRD lines at  $25.70^\circ$  and  $39.94^\circ$  are 0.346 and 0.226 nm, respectively. These results are in good agreement with the HRTEM measurement (0.347 and 0.227 nm) shown in Figure 2. However, the XRD pattern of  $\text{Cu}_3\text{Cl}(\text{SR})_2$  cannot be fitted with any known Cu-compounds in present XRD database and this indicates that

the  $\text{Cu}_3\text{Cl}(\text{SR})_2$  is a new compound that has never been reported before.

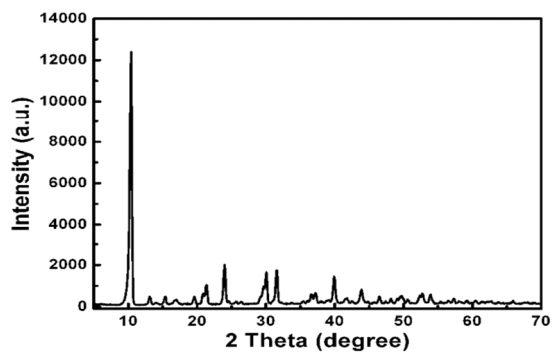


Figure 3. Powder XRD pattern of  $\text{Cu}_3\text{Cl}(\text{SR})_2$ .

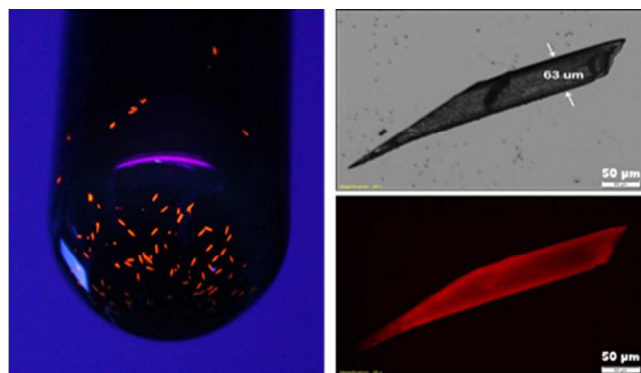


Figure 4. Single crystals of  $\text{Cu}_3\text{Cl}(\text{SR})_2$  with size of about  $60\mu\text{m} \times 60\mu\text{m} \times 450\mu\text{m}$  used in structure analysis. On the left are the crystals emitting red fluorescence excited by a UV lamp; on the right is one crystal imaged by an optical microscope (top right) and a microscope fluorescence image excited at 350 nm (bottom right).

In order to determine the crystal structure of  $\text{Cu}_3\text{Cl}(\text{SR})_2$ , large crystals were grown for single crystal XRD as shown in Figure 4. The crystal size is about  $60\mu\text{m} \times 60\mu\text{m} \times 450\mu\text{m}$  and the luminescence spectra of these crystals are the same as that of the powder samples (see Figure S1 in supporting document). The crystal structure of  $\text{Cu}_3\text{Cl}(\text{SR})_2$  (Figure 5) was determined by single crystal X-ray diffraction. The compound crystallizes in the monoclinic space group  $C2/c$  and the cell parameters are  $a = 7.5510(4)$  Å,  $b = 16.9848(7)$  Å,  $c = 7.8364(4)$  Å,  $\beta = 104.798(3)^\circ$ . Its empirical formula is  $\text{Cu}_3\text{Cl}(\text{SR})_2$  with formula weight 378.38 g/mol. (See details about structure and refinement from Table S1 to S8.) Figure 6 shows the theoretically calculated X-ray diffraction pattern (in red) from the single crystal data and the experimental X-ray diffraction pattern (in black) of the synthesized crystal powders. The powder diffraction pattern is calculated from single crystal X-ray data using the program POUDEX (J. Laugier and B. Bochu, Multiphases version of POUDEX-V2, 2003). The obtained graph for the simulated powder diffraction is exported as a \*.cpi file and converted using PowderX (C. Dong, Institute of Physics, Chinese Academy of Sciences, Beijing, China) into a \*.xrd file, which is used for plotting the powder spectrum using the program Origin7.0 (OriginLab Corp., Northampton, USA). Details on calculated

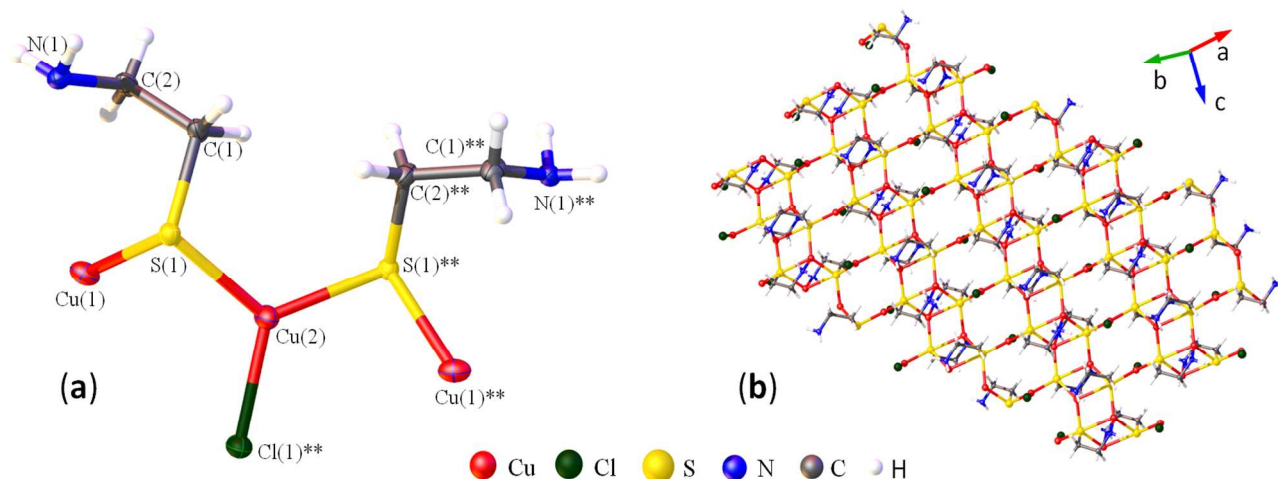


Figure 5. Crystal structure of  $\text{Cu}_3\text{Cl}(\text{SR})_2$ . (a) Molecular ellipsoid plot with selected bond distances ( $\text{\AA}$ ) and angles ( $^\circ$ ): Cu(1)-S(1), 2.3167(9); Cu(2)-S(1), 2.2474(8); Cu(2)-Cl(1), 2.2739(12); S(1)-C(1), 1.839(3); N(1)-C(2), 1.475(4); S(1)\*\*-Cu(2)-S(1), 119.45(4); S(1)-Cu(2)-Cl(1), 120.27(2); C(1)-S(1)-Cu(1), 106.60(11); Cu(2)-S(1)-Cu(1), 92.83(3); C(1)-S(1)-Cu(2), 109.81(11). Symmetry transformations used to generate equivalent atoms: \*\*,  $-x+1, y, -z+\frac{1}{2}$ . (b) One strand as part of the unit cell.

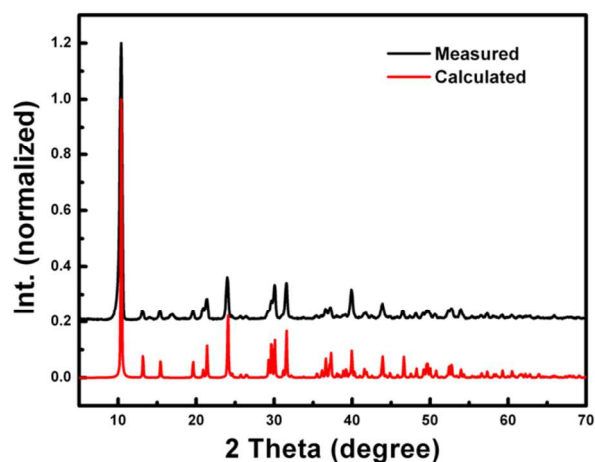


Figure 6. The calculated (red) and measured (black) powder diffraction pattern of  $\text{Cu}_3\text{Cl}(\text{SR})_2$ .

powder diffraction from single crystal X-ray data is provided in supporting information (Table S9). As shown in Figure 6, the calculated pattern matches perfectly to the measured XRD pattern, confirming that the material is  $\text{Cu}_3\text{Cl}(\text{SR})_2$ . The XPS spectroscopy is also performed and reveals significant signals of C, S, N, Cl and Cu in the  $\text{Cu}_3\text{Cl}(\text{SR})_2$  (Figure S2), which is consistent with the composition obtained from single crystal X-ray diffraction measurement. The O displayed in the XPS is due to sample surface O absorbance. The Ag signals are observed because Ag film is used for coating on the surface of a small silicon wafer in XPS sample preparation. The new structure includes two different Cu atoms – Cu(1) and Cu(2) (Figure 5a), which bind to 4 and 3 other atoms respectively (Figure 5b). The valence calculation shows they are both  $\text{Cu}^+$  ions (see Table S10 in supporting information). This is not surprising as excess cysteamine is able to completely reduce  $\text{Cu}^{2+}$  to  $\text{Cu}^+$  ions.<sup>17</sup> In many coordination structures, a thiolate sulfur atom binds less than 4 metal atoms, while in Cu-Cy crystals, the sulfur atom

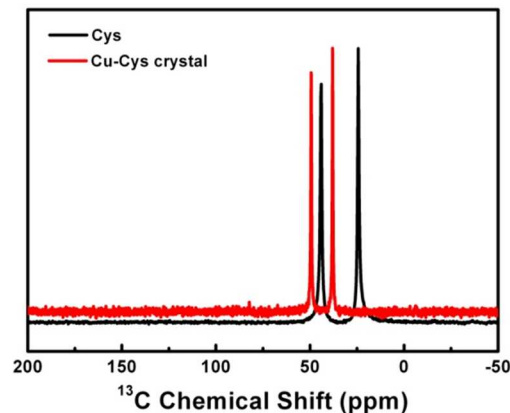


Figure 7. The  $^{13}\text{C}$  CP-MAS spectra of  $\text{Cu}_3\text{Cl}(\text{SR})_2$  crystals (red) and cysteamine (black).

usually bridges 4 Cu atoms simultaneously.<sup>18, 19</sup> This 4-bridge S-Cu bonding is also observed in our case. While the other 3 S-Cu bond lengths are between 2.24  $\text{\AA}$  ~ 2.32  $\text{\AA}$ , one S-Cu bridge is much longer (2.61  $\text{\AA}$ ), which is very different to the previous reported structures (2.22  $\text{\AA}$  ~ 2.48  $\text{\AA}$ ).<sup>18, 19</sup> The new Cu-Cy crystal  $\text{Cu}_3\text{Cl}(\text{SR})_2$  has less atoms in its repeating unit cell than the previously reported Cu-Cy crystals of  $\text{Cu}_{13}\text{Cl}_{13}(\text{SR}')_6$  and  $\text{Cu}_8\text{Cl}_8(\text{SR}')_6$ , where  $\text{R}' = \text{CH}_2\text{CH}_2\text{NH}_3$ .<sup>18, 19</sup> It is noticed that  $\text{SR}'$  is neutral while SR is not. As revealed in Figure 5b, both ends (thiol group and amine group) from SR bond to Cu(1), the thiol group forms a covalence bond with Cu(1) while the electron pair from the amine group forms a coordinate bond with the same atom. In the previous Cu-Cy structures, only thiol groups bond with Cu atoms. Here, the chelating may stabilize the structure. The  $\text{Cu}_3\text{Cl}(\text{SR})_2$  viewed along (100), (010), and (001) direction are displayed in Figure S3, S4, and S5, respectively.

To further probe the oxidation state of Cu in  $\text{Cu}_3\text{Cl}(\text{SR})_2$ ,  $^{13}\text{C}$  CP-MAS spectra of  $\text{Cu}_3\text{Cl}(\text{SR})_2$  and the ligand precursor (cysteamine hydrochloride) were acquired (Figure 7). For the

ligand precursor (HS-C(1)H<sub>2</sub>-C(2)H<sub>2</sub>-NH<sub>2</sub>·HCl), the isotropic chemical shifts of carbon atoms C(1) and C(2) are 24.3 and 43.8 ppm, respectively. Upon formation of Cu<sub>3</sub>Cl(SR)<sub>2</sub>, these two peaks shift to the downfield direction and appear at 38.0 and 49.4

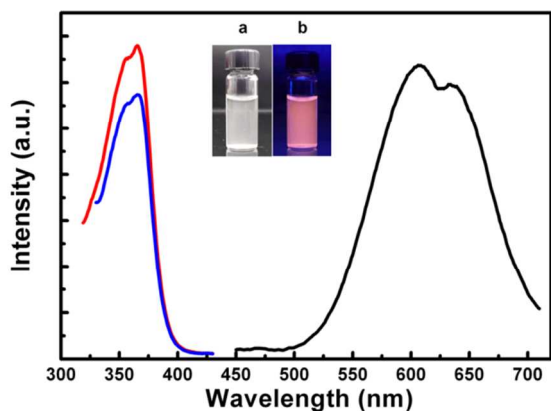


Figure 8. Photoluminescence emission spectra (black) of Cu<sub>3</sub>Cl(SR)<sub>2</sub> following 360 nm excitation. Excitation spectra are shown by monitoring emission of 607 nm (red) and 633 nm (blue) respectively. The insets (a) and (b) display the photos of Cu<sub>3</sub>Cl(SR)<sub>2</sub> in water and their photoluminescence under white light and UV lamp (360 nm) respectively.

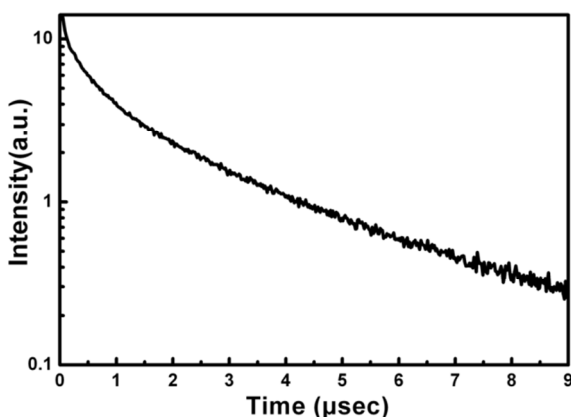


Figure 9. The luminescence lifetime of Cu<sub>3</sub>Cl(SR)<sub>2</sub>. A double exponential decay equation  $I = I_1 \exp(-t/t_1) + I_2 \exp(-t/t_2)$  fits the decay curve very well, where  $I$  represents the intensity,  $I_1$ ,  $t_1$ ,  $I_2$ , and  $t_2$  are 6.19, 1.82, 7.77, and 0.21, respectively.

ppm. The observation that the carbon atom C(1) exhibits a significantly larger shift is indicative of the copper ion bound to the sulfur atom. The facts that the observed shifts of the ligand precursor are small (less than 15 ppm) upon coordination and that no spinning side bands are observed at the relatively low spinning speed used for Cu<sub>3</sub>Cl(SR)<sub>2</sub> suggest that the Cu ion is a diamagnetic species (i.e. Cu<sup>+</sup>). Thus, the NMR data are consistent with single-crystal XRD results that the oxidation state of copper in Cu<sub>3</sub>Cl(SR)<sub>2</sub> is +1, rather than +2.

The Cu<sub>3</sub>Cl(SR)<sub>2</sub> displays intense photoluminescence and X-ray luminescence, while many copper complexes have no luminescence due to efficient internal conversion.<sup>21, 22</sup> The photoluminescence remains constant when Cu<sub>3</sub>Cl(SR)<sub>2</sub> was

suspended in a solution with a wide range of pH values (5 to 14). Figure 8 shows the photoluminescence emission and excitation spectra of these crystals suspended in water. The inset photos in

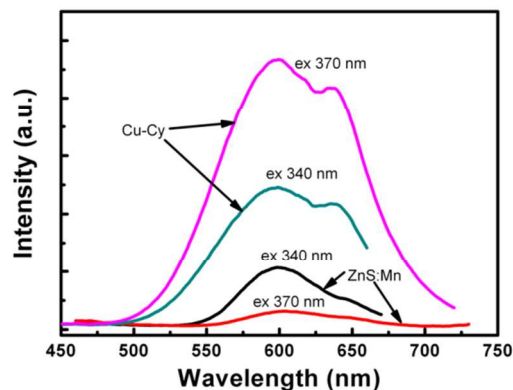


Figure 10. Photoluminescence spectra of Cu<sub>3</sub>Cl(SR)<sub>2</sub> and ZnS:Mn excited at 340 and 370 nm, respectively.

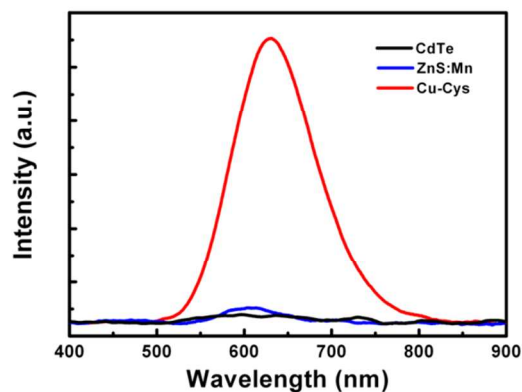


Figure 11. The X-ray luminescence spectra of Cu<sub>3</sub>Cl(SR)<sub>2</sub>, ZnS:Mn and CdTe.

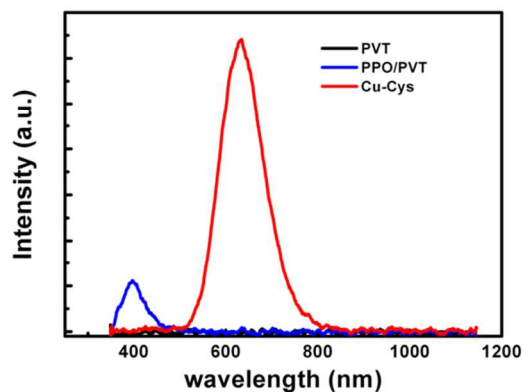


Figure 12. X-ray excited luminescence spectra of Cu<sub>3</sub>Cl(SR)<sub>2</sub>, PVT and PVT/PPO with same volume.

Figure 8 display Cu<sub>3</sub>Cl(SR)<sub>2</sub> in water under white light (inset a) and UV lamp (360 nm, inset b) excitation. Two red emissions peaking at 607 nm and 633 nm are observed from these crystals,

indicating two luminescence emitting centres. For luminescence of metal complexes, metal-to-ligand charge transfer (MLCT)<sup>23-26</sup> and ligand-to-metal charge transfer (LMCT)<sup>27, 28</sup> transitions play an important role. Meanwhile, other mechanisms also exist<sup>29, 30</sup> and the emission of Cu-complex crystals from metal centred (MC) excited states has been reported.<sup>30</sup> Here, as Cu<sup>+</sup> is rather reducing than oxidizing and has fully filled with d-shell (d<sup>10</sup>), MLCT but not LMCT transitions would be expected. However, the cysteamine ligand is saturated and has no low-lying empty orbitals, which would make the MLCT also not allowed. In this view, we suggest that the luminescence of Cu<sub>3</sub>Cl(SR)<sub>2</sub> corresponds to the Cu MC transition (- d<sup>9</sup>4s<sup>1</sup> - d<sup>10</sup>), which can be strongly affected by Cu - Cu interactions.<sup>30</sup> It is reasonable

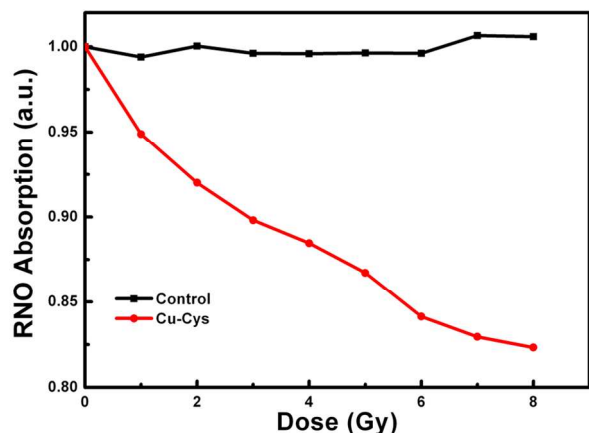


Figure 13. RNO absorption quenched by singlet oxygen produced in control, Cu<sub>3</sub>Cl(SR)<sub>2</sub> using X-ray irradiation.

seeing the two emission peaks from Cu<sub>3</sub>Cl(SR)<sub>2</sub> since there are two type of copper ions - Cu(1) and Cu(2), which are differed from each other by different coordinations. The Cu<sup>+</sup> excited state (d<sup>9</sup>4s<sup>1</sup>) may be strongly contracted and distorted by an increase of Cu - Cu interaction.<sup>30</sup> Thus, the longer wavelength (633 nm) emission is likely related to Cu(1) as its shorter distances to neighbourhood copper ions (2.81 Å and 2.89 Å), compared to the distances of Cu(2) and its neighbourhood copper ions (3.31 Å and 3.74 Å). Consequently, the 607 nm emission is assigned to Cu(2) ions. The luminescence lifetime of Cu<sub>3</sub>Cl(SR)<sub>2</sub> is plotted in Figure 9. The lifetime curve fits a double exponential function well, with t<sub>1</sub> = 1.82 μs and t<sub>2</sub> = 0.21 μs. The observed lifetimes may be due to different environment of copper ions. However, the overlapping nature of the transitions precludes making a definitive assignment based on the lifetime analysis alone.

ZnS:Mn is a well-known phosphor that has been used for solid state lighting and displays.<sup>31-35</sup> To compare the luminescence efficiency of Cu<sub>3</sub>Cl(SR)<sub>2</sub> with that of ZnS:Mn, measurements were done on the same amount of samples under the same conditions. As shown in Figure 10, the photoluminescence of Cu<sub>3</sub>Cl(SR)<sub>2</sub> is 2.5 times stronger in intensity than that of ZnS:Mn when excited at 340 nm, and is about 15 times stronger when excited at 370 nm for the same volume of samples that were measured under the same conditions. Different excitation wavelengths are used for emission intensity comparison as the two materials may not have same best excitation wavelength (340 nm for ZnS:Mn and 370

nm for Cu<sub>3</sub>Cl(SR)<sub>2</sub>). As an overall observation, the Cu<sub>3</sub>Cl(SR)<sub>2</sub> has more intensive luminescence than ZnS:Mn. The Cu<sub>3</sub>Cl(SR)<sub>2</sub> also has intense X-ray excited luminescence as shown in Figures 11, 12 and S6. Semiconductor quantum dots like CdTe and ZnS:Mn<sup>35, 36</sup> have been proposed and investigated as potential materials for radiation detection. However, they exhibit only very weak X-ray luminescence (Figure 11), when measured under the same conditions as the intensely luminescent Cu<sub>3</sub>Cl(SR)<sub>2</sub>. The X-ray luminescence of Cu<sub>3</sub>Cl(SR)<sub>2</sub> is about 10 times stronger in intensity than that of ZnS:Mn and about 35 times stronger than that of CdTe quantum dots. The X-ray luminescence (the emission band area) of Cu<sub>3</sub>Cl(SR)<sub>2</sub> is much stronger than that of polyvinyl toluene (PVT)/ 2,5-Diphenyloxazole (PPO) as shown in Figures 12 and S6. It should be noted that the volume of Cu<sub>3</sub>Cl(SR)<sub>2</sub> crystals is only 1% in volume in the composites but their X-ray luminescence is even stronger than that of the undoped PVT/PPO polymer (see Figure S6). This indicates that Cu<sub>3</sub>Cl(SR)<sub>2</sub> has much higher X-ray luminescence quantum efficiency than that of PVT/PPO. Figure 12 compares the X-ray luminescence of PVT, PVT/PPO and Cu<sub>3</sub>Cl(SR)<sub>2</sub> at the same volume and the results show that the intensity of X-ray luminescence of Cu<sub>3</sub>Cl(SR)<sub>2</sub> is 5 times stronger than that of PVT/PPO. All these results indicate that Cu<sub>3</sub>Cl(SR)<sub>2</sub> is a new and promising scintillator for radiation detection and dosimetry. It is also noted that the new Cu<sub>3</sub>Cl(SR)<sub>2</sub> compound displays intense scintillation luminescence centred at 633 nm by X-ray excitation, which is different from the photoluminescence peak at 607 nm. This suggests that X-ray luminescence of Cu<sub>3</sub>Cl(SR)<sub>2</sub> is related to different coordinations of copper ions.

In the last, it should be pointed out that Cu<sub>3</sub>Cl(SR)<sub>2</sub> can be used as a new type of photosensitizers that can be used for cancer treatment. It is very interesting that the Cu<sub>3</sub>Cl(SR)<sub>2</sub> can produce singlet oxygen upon irradiation by X-ray as shown in Figure 13. This means that the Cu<sub>3</sub>Cl(SR)<sub>2</sub> particles not only can be used for skin cancer treatment but also can be used for deep cancer treatment since X-ray can penetrate deeply into tissue. The potential impact of the reported Cu<sub>3</sub>Cl(SR)<sub>2</sub> would be tremendous and it is further expected to get into market helping cancer fighters. Details are reported in our forthcoming paper.<sup>20</sup>

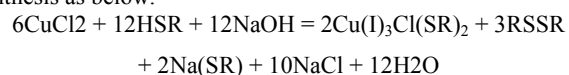
## Conclusions

In summary, the structure and optical properties of a new Cu-Cysteamine complex with a formula of Cu<sub>3</sub>Cl(SR)<sub>2</sub> are reported. The Cu<sub>3</sub>Cl(SR)<sub>2</sub> has a new structure in which both thio and amine groups from cysteamine bond with copper ions. Both the single-crystal X-ray diffraction and the solid-state nuclear magnetic resonance results show that the oxidation state of copper in the Cu<sub>3</sub>Cl(SR)<sub>2</sub> is +1, rather than +2. The new Cu-complex has intense photoluminescence and X-ray luminescence and holds applications in various fields, such as lighting, fluorescence imaging, radiation detection, and light source for photodynamic activation. More interestingly, Cu<sub>3</sub>Cl(SR)<sub>2</sub> as a new type of photosensitizer that not only can be activated by light for skin cancer treatment but also can be activated by X-ray for deep cancer treatment.

## Experimental

## Chemicals and Synthesis

Copper(II) chloride dihydrate (99.99%), 2-Mercaptoethylamine hydrochloride (Cysteamine hydrochloride or Cys, 98%) and Sodium hydroxide (98%) were purchased from Sigma (USA). All the chemicals were used as received. Deionized (DI) water was used as the reaction solvent without further purification. For synthesis of the Cu-complex,  $\text{CuCl}_2 \cdot 2\text{H}_2\text{O}$  (0.460 g, 2.698 mmol,) was dissolved in DI water followed by addition of cysteamine (0.636 g, 8.244 mmol). With excessive cysteamine, the  $\text{Cu}^{2+}$  (Cu(II)) were completely reduced to  $\text{Cu}^+$  (Cu(I)), expressed as  $2\text{HSR} + \text{Cu(II)} = \text{Cu(I)-SR} + \frac{1}{2} \text{RSSR} + 2\text{H}^+$ . After adjusting the pH value to 8 by adding a 2.5 M NaOH solution, the solution was stirred for about 2 h at room temperature till it turned to deep violet due to oxidation. An intermediate product consist of both Cu(I) and Cu(II) was suggested for causing the violet colour and assumed in a form of  $\text{Cu(II)}_2(\text{SR})_2\text{OCu(I)}_4(\text{SR})_4$ . Further investigation of the intermediate product would be continued in the future. The solution was then heated to its boiling temperature for 30 min. Crystals of  $\text{Cu}_3\text{Cl}(\text{SR})_2$  were precipitated from the solution and other reaction products were removed with supernatant. The obtained  $\text{Cu}_3\text{Cl}(\text{SR})_2$  crystals were further centrifuged and washed using a mixture of DI water and ethanol ( $v/v = 5:4$ ) for three times. Finally, the crystals were dried completely in a vacuum oven at room temperature overnight. The large single crystals were obtained for longer time with no stirring. We suggest an overall reaction for the  $\text{Cu}_3\text{Cl}(\text{SR})_2$  synthesis as below.



## Scanning electron microscopy (SEM) and transmission electron microscopy (TEM)

The obtained  $\text{Cu}_3\text{Cl}(\text{SR})_2$  was dispersed in water and loaded onto a Cu substrate. After drying completely, the sample was observed by a Hitachi S-5000H field emission scanning electron microscope. For TEM measurement, the  $\text{Cu}_3\text{Cl}(\text{SR})_2$  dispersed in water was ground and sonicated before placed onto holey carbon-covered copper grids for HRTEM observations. The HRTEM images of the particles were obtained with a Hitachi 9500 electron microscope with accelerating voltage of 300 kV.

## Solid-state Nuclear Magnetic Resonance (NMR) Spectroscopy

$^{13}\text{C}$  CP-MAS spectra of  $\text{Cu}_3\text{Cl}(\text{SR})_2$  and the ligand precursor cysteamine hydrochloride were acquired on a Varian/Chemagnetics Infinityplus 9.4 T WB spectrometer and a 21.1 T Bruker Avance II spectrometer, respectively. All the  $^{13}\text{C}$  CP-MAS spectra were obtained at room temperature with a contact time of 1 ms and a pulse delay of 5 s. The sample spinning rates were 8 and 10 kHz for  $\text{Cu}_3\text{Cl}(\text{SR})_2$  and cysteamine hydrochloride, respectively.  $^{13}\text{C}$  chemical shifts were referenced externally to the resonance of the methylene carbon in adamantane (38.55 ppm relative to TMS).

## Single Crystal X-ray Diffraction

A pale brown rod-like crystal of  $\text{Cu}_3\text{Cl}(\text{SR})_2$  having the approximate dimensions of  $0.10 \times 0.03 \times 0.03$  mm, coated with oil (Paratone 8277, Exxon), was collected onto the elongated aperture of a mounted MicroLoop E<sup>TM</sup> (diameter of the aperture:

100 microns; *MiTeGen* - Microtechnologies for Structural Genomics; USA). The crystal was then mounted onto the goniometer head, which was quickly transferred to the cold stream of the Oxford cryo-jet. The mounted MicroLoop<sup>TM</sup> had previously been attached reusable goniometer bases consisting of stainless steel magnetic base and a copper post extending up from the stainless steel base. The MicroLoop<sup>TM</sup> is grabbed and securely held in reusable goniometer bases without using epoxy.

All measurements were made on a Nonius KappaCCD 4-Circle Kappa FR540C diffractometer using monochromated Mo  $\text{K}\alpha$  radiation ( $\lambda = 0.71073$  Å) at  $-100$  °C. An initial orientation matrix and cell was determined from 10 frames using  $\omega$  scans and the data were measured using  $\omega$ -scans.<sup>37</sup> A total of 2662 reflections were collected. Cell parameters were initially retrieved using the COLLECT<sup>37</sup> software, refined with the HKL DENZO and SCALEPACK software using 1355 observed reflections with  $1.00^\circ < \theta < 30.03^\circ$  (mosaicity:  $0.428(3)^\circ$ ) from the data collection, and corresponded to a monoclinic cell. Data reductions were performed with the HKL DENZO and SCALEPACK software,<sup>38</sup> which corrects for beam inhomogeneity, possible crystal decay, Lorentz and polarization effects. A multi-scan absorption correction was applied (SCALEPACK).<sup>38</sup> The crystal structures were solved using the heavy atoms method (Patterson)<sup>39</sup> and refined by full-matrix least-squares method on  $F^2$  with SHELXL-2012.<sup>40</sup> The non-hydrogen atoms were refined anisotropically. Hydrogen atoms were included at geometrically idealized positions and were not refined. The isotropic thermal parameters of these hydrogen atoms were fixed at 1.2 or 1.5 times that of the preceding carbon or nitrogen atom, respectively. Neutral atom scattering factors for non-hydrogen atoms and anomalous dispersion coefficients are contained in the SHELXL-2012 program.<sup>40</sup> Further details for the determination of crystal structures are given in the supporting information. Molecular thermal ellipsoid plots were prepared using OLEX-2 for Windows.

## X-ray powder diffraction (XRD) and photoelectron spectroscopy (XPS)

The obtained  $\text{Cu}_3\text{Cl}(\text{SR})_2$  powders were measured by X-ray diffraction recorded in a Rigaku Ultima IV X-ray diffractometer with a Cu K-alpha source of  $\lambda = 1.5406$  Å. For XPS measurement, the  $\text{Cu}_3\text{Cl}(\text{SR})_2$  powders were ground and dispersed in water and deposited on the surface of a silver coated silicon wafer. After sample drying in a vacuum oven at  $40$  °C overnight, the XPS survey and quantification report were then carried out by using a Perkin-Elmer PHI 560 high performance spectrometer.

## Absorption, photoluminescence and lifetimes

The absorption and photoluminescence spectra were measured using a Shimadzu UV-2450 UV-Vis spectrophotometer and a Shimadzu RF-5301PC fluorescence spectrophotometer (Kyoto, Japan), respectively. The Luminescence lifetimes were collected using a nanosecond optical parametric oscillator/amplifier (Spectra-Physics MOPO-730) operating at a 10 Hz repetition rate and tunable between 440 and 1800 nm. The output of the MOPO system was frequency doubled in a KDP crystal and directed onto the particles. Emission was collected at right angles to the excitation and focused into a 1/8-meter monochromator equipped

with a standard photomultiplier tube.

### X-ray luminescence measurement

The X-ray luminescence spectrum was measured in a light-proof X-ray cabinet equipped with fiber optic connection to an outside detector. The X-ray Irradiation was performed using a Faxitron RX-650 (Faxitron X-ray Corp, IL, USA) at 90 kV with a 12 inch mm source-object distance and 5 mm distance optic fiber to object, at 45°. The luminescence spectra were recorded using a QE65000 spectrometer (Ocean Optics Inc., Dunedin, FL), connected to the X-ray chamber using a 0.6 mm core diameter optic fiber (P600-2-UV-V is, Ocean Optics Inc, Dunedin, FL), which has a probe head extended inside the X-ray chamber and positioned at 45° and 5 mm away from sample surface.

### Singlet oxygen measurement

A p-nitrosodimethylaniline(RNO)-imidazole(ID) method<sup>41</sup> was applied to detect singlet oxygen generated in water under different X-ray irradiation. RNO is a water-soluble molecule with absorption that can be quenched irreversibly by singlet oxygen in the presence of ID.<sup>41</sup> Briefly, 0.225 mg RNO and 16.34 mg ID were added in 30 ml DI water, which was air saturated by sufficient air bobbling. The sample solution of Cu<sub>3</sub>Cl(SR)<sub>2</sub> was prepared by adding 1 mg of Cu<sub>3</sub>Cl(SR)<sub>2</sub> into 3 ml above RNO-ID solution. Then, the RNO-ID solution (as control) and Cu<sub>3</sub>Cl(SR)<sub>2</sub> solution were exposed under different X-ray doses (0 ~ 8 Gy) using a Faxitron RX-650 cabinet X-ray system (Faxitron X-ray LLC, USA). Meanwhile, the intensity of RNO absorption peak at 440 nm of different solutions was monitored by a Shimadzu UV-vis spectrophotometer.

### Acknowledgements

We would like to acknowledge the support from the U.S. Army Medical Research Acquisition Activity (USAMRAA) under Contracts of W81XWH-10-1-0279 and W81XWH-10-1-0234 and partially the NSF and DHS joint ARI program (2011-DN-077-ARI053-02, 3&4).

### Notes and references

<sup>a</sup> Department of Physics and the SAVANT Center, The University of Texas at Arlington, Arlington, Texas 76019-0059, USA. E-mail: weichen@uta.edu

<sup>b</sup> Saskatchewan Structural Sciences Centre, University of Saskatchewan, Saskatoon, SK S7N 5C9, Canada.

<sup>c</sup> Department of Chemistry, University of Western Ontario, Canada.

<sup>d</sup> Pacific Northwest National Laboratory, Richland, WA 99352, USA.

† Electronic Supplementary Information (ESI) available: Figure S1-S5, X-ray crystallographic files in CIF format, table of crystal data and structure refinement, and table of selected bond distances and angles. See DOI: 10.1039/b000000x/

- S. S. Gupta, M. Stadler, C. A. Noser, A. Ghosh, B. Steinhoff, D. Lenoir, C. P. Horwitz, K.-W. Schramm and T. J. Collins, *Science*, 2002, **296**, 326-328.
- I. Beletskaya, V. S. Tyurin, A. Y. Tsvivadze, R. Guillard and C. Stern, *Chemical Reviews*, 2009, **109**, 1659-1713.
- T. Büttner, J. Geier, G. Frison, J. Harmer, C. Calle, A. Schweiger, H. Schönberg and H. Grützmacher, *Science*, 2005, **307**, 235-238.

- R. N. Patel, K. K. Shukla, A. Singh, M. Choudhary, U. K. Chauhan and S. Dwivedi, *Inorganica Chimica Acta*, 2009, **362**, 4891-4898.
- R. MASON, *Nature* 1968, **217** 543-545.
- J. Chin, S. S. Lee, K. J. Lee, S. Park and D. H. Kim, *Nature*, 1999, **401**, 254-257.
- R. V. Parish, *Metal-Based Drugs*, 1999, **6**, 271-276.
- B. Shapiro and L. Eldjam, *Radiation Research*, 1955, **3**, 393-399.
- J. G. Thoene, R. G. Oshima, J. C. Crawhall, D. L. Olson and J. A. Schneider, *The Journal of Clinical Investigation*, 1976, **58**, 180-189.
- D. C. Jicha and D. H. Busch, *Inorganic Chemistry*, 1962, **1**, 878-883.
- D. C. Jicha and D. H. Busch, *Inorganic Chemistry*, 1962, **1**, 872-877.
- C. H. Wei and L. F. Dahl, *Inorganic Chemistry*, 1970, **9**, 1878-1887.
- R. E. DeSimone, T. Ontko, L. Wardman and E. L. Blinn, *Inorganic Chemistry*, 1975, **14**, 1313-1316.
- D. Habibi, E. Ghaemi and D. Nematollahi, *Molecules*, 2000, **5**, 1194-1200.
- M. S. Bharara, C. H. Kim, S. Parkin and D. A. Atwood, *Polyhedron*, 2005, **24**, 865-871.
- M. S. Bharara, S. Parkin and D. A. Atwood, *Inorganic Chemistry*, 2006, **45**, 7261-7268.
- B. A. Matrana, W. R. Bordelon and D. G. Davis, *Analytical Letters*, 1971, **4**, 437-444.
- R. V. Parish, Z. Salehi and R. G. Pritchard, *Angewandte Chemie International Edition in English*, 1997, **36**, 251-253.
- Z. Salehi, R. V. Parish and R. G. Pritchard, *Journal of the Chemical Society, Dalton Transactions*, 1997, **0**, 4241-4246.
- L. Ma, X. Zou and W. Chen, *Journal of Biomedical Nanotechnology*, 2014, **10**, XXXX (in press)
- M. M. Zulu and A. J. Lees, *Inorganic Chemistry*, 1989, **28**, 85-89.
- Z. Wang and A. J. Lees, *Inorganic Chemistry*, 1993, **32**, 1493-1501.
- R. M. Williams, L. D. Cola, F. Hartl, J. J. Lagref, J. M. Planeix, A. D. Cian and M. W. Hosseini, *Coordination Chemistry Reviews*, 2002, **230**, 253-261.
- Y.-M. Wang, F. Teng, Y.-B. Hou, Z. Xu, Y.-S. Wang and W.-F. Fu, *Applied Physics Letters*, 2005, **87**, 233512-233513.
- S. Supriya and S. K. Das, *Inorganic Chemistry Communications*, 2003, **6**, 10-14.
- H. Kunkely and A. Vogler, *Chemical Physics Letters*, 2003, **368**, 49-52.
- D. M. Knotter, G. Blasse, J. P. M. Van Vliet and G. Van Koten, *Inorganic Chemistry*, 1992, **31**, 2196-2201.
- A. VOGLER and H. KUNKELY, *Inorganica Chimica Acta*, 1981, **53**, L215-L216
- G. Hu, G. J. Mains and E. M. Holt, *Inorganica Chimica Acta*, 1995, **240**, 559-565.
- A. Vogler and H. Kunkely, *Journal of the American Chemical Society*, 1986, **108**, 7211-7212.
- H. E. Gumlich, *Journal of Luminescence*, 1981, **23**, 73-99.
- W. Chen, J. Z. Zhang and A. G. Joly, *J Nanosci Nanotechnol*, 2004, **4**, 919-947.
- W. Chen, A. G. Joly and J. Z. Zhang, *Phys. Rev. B*, 2001, **64**, 412021-412024.
- L. Ma and W. Chen, *J. Appl. Phys.*, 2010, **107**, 123513.

- 
35. M. Hossu, R. O. Schaeffer, L. Ma, W. Chen, Y. Zhu, R. Sammynaiken and A. G. Joly, *Opt. Mater.*, 2013, **35**, 1513-1519.
36. S. E. Letant and T.-F. Wang, *Nano Lett.*, 2006, **6**, 2877.
37. in *COLLECT data collection software*, Nonius B.V., Delft, The Netherlands, 1998.
38. Z. Otwinowski and W. Minor, *Macromolecular Crystallography, Part A*, Carter, C. W., Jr., Sweet, R. M., Eds.; Academic Press: San Diego, CA, , 1997, **276**, 307-326.
39. G. M. Sheldrick, *University of Göttingen, Göttingen, Germany 1997*. G. M. Sheldrick, *Acta crystallographica*, 1997, **A64**, 112-122.
40. G. M. Sheldrick, *University of Göttingen, Göttingen, Germany 2013*. G. M. Sheldrick, *Acta crystallographica*, 2008, **A64**, 112-122.
41. I. Kraljić and S. E. Mohsni, *Photochemistry and Photobiology*, 1978, **28**, 577-581.